Why not record from *every* electrode with a CMOS scanning probe?

George Dimitriadis[†, 1, *], Joana P. Neto[1, 8, 18, *], Arno Aarts[2], Andrei Alexandru[3], Marco Ballini[3], Francesco Battaglia[4], Lorenza Calcaterra[1], Susu Chen[23, 24], Francois David[5], Richárd Fiáth[6, 7], João Frazão[8], Jesse P Geerts[1], Luc J. Gentet[5], Nick Van Helleputte[3], Tobias Holzhammer[2], Chris van Hoof[3], Domonkos Horváth[6, 7, 9], Gonçalo Lopes[1], Carolina M. Lopez[3], Eric Maris[4], Andre Marques-Smith[1], Gergely Márton[6, 7], Bruce L. McNaughton[19, 20], Domokos Meszéna[6, 7], Srinjoy Mitra[10], Silke Musa[3], Hercules Neves[11, 17], Joana Nogueira[1], Guy A. Orban[12], Frederick Pothof[13], Jan Putzeys[3], Bogdan Raducanu[3, 14], Patrick Ruther[13, 21], Tim Schroeder[4], Wolf Singer[15], Nicholas A. Steinmetz[22], Paul Tiesinga[16], Istvan Ulbert[6, 7], Shiwei Wang[3], Marleen Welkenhuysen[3], Adam R. Kampff[1]

†g.dimitriadis@ucl.ac.uk

* These authors contributed equally to this work

1) Sainsbury Wellcome Centre for Neural Circuits and Behaviour, University College London, United Kingdom
2) ATLAS Neuroengineering, Leuven, Belgium
3) imec, 3001 Leuven, Belgium
4) Donders Institute for Brain, Cognition and Behavior, Radboud University Nijmegen, The Netherlands
5) Team Waking, Lyon Neuroscience Research Center (CNRL), INSERM-U1028, CNRS-UMR5292, Bron, France
6) Institute of Cognitive Neuroscience and Psychology, Research Centre for Natural Sciences, Hungarian Academy of Sciences, Budapest, Hungary
7) Faculty of Information Technology and Bionics, Pazmany Peter Catholic University, Budapest, Hungary
8) Champalimaud Neuroscience Programme, Champalimaud Centre for the Unknown, Portugal
9) School of PhD Studies, Semmelweis University, Budapest, Hungary
10) Institute for Integrated Micro and Nano Systems (IMNS), University of Edinburgh, UK
11) Uppsala University, Sweden
12) Department of Medicine and Surgery, University of Parma, Parma, Italy
13) Department of Microsystems Engineering (IMTEK), University of Freiburg, Germany
14) Electrical Engineering Department-ESAT, KU Leuven, 3001 Leuven, Belgium
15) ErnstStrüngmann Institute for Neuroscience in Cooperation with Max Planck
16) Neurinformatics department, Donders Institute for Brain, Cognition and Behavior, Radboud University Nijmegen, Heyendaalseweg 135, 6525 AJ, Nijmegen, The Netherlands
17) Fiocruz, Brazil
18) Departamento de Ciência dos Materiais, CENIMAT/I3N and CEMOP/Uninova, Faculdade de Ciências Tecnologia−Universidade Nova de Lisboa, Caparica, Portugal
19) Department of Neurobiology and Behavior, University of California at Irvine, Irvine CA, USA, 92697-8439
20) Department of Neuroscience, The University of Lethbridge, Lethbridge, AB, Canada, T1K 3M4
21) Cluster of Excellence BrainLinks-BrainTools, University of Freiburg, Germany
22) Department of Biological Structure, University of Washington, Seattle, WA
23) University College London

24) Janelia Research Campus, HHMI

Abstract

It is an uninformative truism to state that the brain operates at multiple spatial and temporal scales, each with each own set of emergent phenomena. Yet, a point, more worthy of attention, is the fact that our current understanding of it cannot clearly point to which of these phenomenological scales are the significant contributors to the brain's function and primary output (i.e. behaviour). Apart from the seer complexity of the problem, a major contributing factor to this state of affairs is the lack of instrumentation that can address multiple scales at once without causing function altering damages to the underlying tissue. One facet of this problem is the fact that standard neural recording devices normally require one output connection per electrode. This limits the number of electrodes that can fit along the thin shafts of implantable probes generating a limiting balance between density and spread. Sharing a single output connection between multiple electrodes relaxes this constraint and permits designs of ultra-high density probes.

Here we report the design and in-vivo validation of such a device, a complementary metal-oxide-semiconductor (CMOS) scanning, 1344 electrodes, probe; the outcome of the European research project NeuroSeeker. We show that this design targets both local and global spatial scales by allowing the simultaneous recording of more than 1000 neurons spanning 7 functional regions with a single shaft. The neurons show similar recording longevity and signal to noise ratio to passive probes of comparable size and no adverse effects in awake or anesthetized animals. Addressing the data management of this device we also present novel visualization and monitoring methods.

To help design electrode configurations for future, even higher density, CMOS probes, recordings from many different brain regions were obtained with an ultra-dense passive probe.

Introduction

The number of neurons that can be monitored simultaneously during an extracellular recording is currently limited by the number of electrodes that can be implanted (Stevenson, 2017; Stevenson and Kording, 2011). However, the desire for large-scale monitoring of single neuron activity and the need to minimize tissue damage compete with one another (Buzsáki et al., 2015). The high resolution processes of semiconductor fabrication (i.e., photolithographic patterning of thin film conductors and insulators on a silicon substrate) have enabled dozens of microelectrodes, packed with an ever increasing density, along needle-like probes (Blanche et al., 2005; Dugué et al., 2011; Torfs et al., 2011; Berenyi et al., 2014; Buzsáki et al., 2015; Shobe et al., 2015; Herbawi et al., 2018; Dorigo et al., 2018). In the standard "passive" silicon probe, electrodes distributed along the probe shaft must each be connected to an external contact pad on the probe base by metal lines deposited along the shaft. Advances in lithography techniques (i.e., e-beam lithography (Rios et al., 2016; Scholten and Meng, 2016)), metal deposition procedures, and quality control have made it possible to fabricate a five shank, 1000-channel probe, where each shank (width of ~50 µm) has 200 electrodes of 9 × 9 µm and a pitch of 11 µm (Scholvin et al., 2016). Despite these impressive designs, a bottleneck remains in the number of output connection lines that can be squeezed into a single, thin probe shaft. Therefore, monitoring the thousands of electrodes required to densely cover an 8 mm x 100 µm probe will demand a new technology; a technology that multiplexes the signal from multiple electrodes into one output line.

The semiconductor industry has solved the same interconnect challenge with integrated circuitry (IC), often fabricated using the CMOS manufacturing process. As a characteristic example, mobile

phones with on-board cameras use CMOS image sensors (CIS) that are lightweight and low power, but that can convert an optical image into an electronic signal with very high spatial resolution. A CIS is composed of an array of millions of identical pixels, each having at least a photodiode, an addressing transistor that acts as a switch, and an amplifier. Each pixel is sampled once within each frame and the image output is generated by rapidly scanning the full sensor matrix. This active switching / time multiplexing is crucial for achieving the small size of a CIS device, as it conveys the signals from many pixels with just a few output connections.

In the case of silicon probes, their one-dimensional architecture, high sampling speed requirements (three orders of magnitude larger than a CIS), the low amplitude of the neural signals (three orders of magnitude lower than the photodiode signals in CMOS cameras) and the need to avoid tissue overheating due to electrical power dissipation have challenged the inclusion of integrated circuitry within the probe's shaft. The concept of integrating electronic elements in the same substrate used to build the recording electrodes was first introduced in the 1980s (Najafi and Wise, 1986; Najafi et al., 1985; Wise and Ji, 1992; Wise and Najafi, 1991) The most recent CMOS-based implantable probe designs for *in vivo* applications integrate circuitry into both the probe base and within the probe shaft(s) and have been reviewed elsewhere (Lopez et al., 2013, 2016; Obien et al., 2015; Ruther and Paul, 2015; Raducanu et al., 2016; Seymour et al., 2017; Steinmetz et al., 2018).

The NeuroSeeker European research project aimed to produce CMOS-based, time multiplexing, silicon probes for extracellular electrophysiological recordings with 1344 electrodes on a 50 µm thick, 100 µm wide, and 8 mm long shank with a 20 x 20 µm electrode size and a pitch of 22.5 µm (see Box 1 for a technical overview of the probe and (Raducanu et al., 2016, 2017) for an in depth description of the probe's design). This innovative solution has allowed the neuroscientists within the consortium to record brain activity with an unprecedented combination of resolution and scale. Here we report the use of the NeuroSeeker probe to record from both anesthetized and freely moving rats. We characterize in saline and *in vivo* the increase in noise that the local amplification and time multiplexing scheme incurs relative to a passive electrode probe with the same configuration. We show that this increase is insignificant *in vivo* and does not inhibit the capture of high quality neural signals. In the case of freely moving animals, we also include data showing that the signal remains stable for at least 10 days. We also describe a method for removing the NeuroSeeker probe intact, and ready for reuse, from the brain of a chronically implanted animal and show results from freely moving recordings from an animal implanted with such a 'second hand' probe. This allows the multiple re-use of probes whose price, and low production numbers, makes them currently inaccessible to all but a tiny minority of electrophysiology labs around the world. Finally, we show how probes that span multiple areas can capture brain behaviour around salient moments of an animal's behaviour that would be missed by probes with smaller brain coverage. We then compare the NeuroSeeker signal with signals of equal spread but sparser electrode distributions and showcase how non CMOS probe have to choose between capturing large spatial scale brain activity or accessing detailed knowledge of local activity but not both.

Recording with this number of electrodes results in datasets of around 200 GB per hour with spike numbers in the millions. This scale of data poses new difficulties in the visualization, pre-processing, and curation of the signal, even before it can be used to explore correlations with sensory stimuli or behaviour. Here we present an online visualization method that allows for the rapid overview of the signal from all 1344 electrodes, giving the experimenter a global picture of the recording quality as data is acquired.

Given that CMOS probes with local amplification and time multiplexing allow a significant increase in electrode density without sacrificing compactness, the neuroscientific community must now determine the physiologically relevant limit for the size and density of the electrodes on such

probes. To help address this question, we have collected datasets from ultra-high density (256 electrodes of 5 x 5 µm size with a 6 µm pitch) passive probes. These were recorded from anesthetized rats in a wide range of brain structures and probe orientations. These datasets are available online for further analysis of the optimal geometries for future CMOS probes.

Box 1. NeuroSeeker CMOS-based probe.

The NeuroSeeker probe contains 1344 small electrodes (20×20 µm) with 2.5 µm spacing and 12 larger reference electrodes (40×80 µm).

Time division multiplexing within the shank allows 8 electrode outputs on a single output connection. If a single metal line can be shared by several electrodes, we are no longer restrained by the number of metal lines that can fit within the cross-section of a shank or by the size of the bonding interface in the probe base.

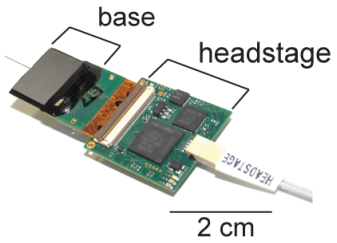

The challenge in such a design is fitting all the required electronics within the electrode area, while making sure the power dissipation is sufficiently low for tissue safety. Due to the high impedance of the electrode, each requires its own amplifier to drive the multiplexed output line (Obien et al., 2015).

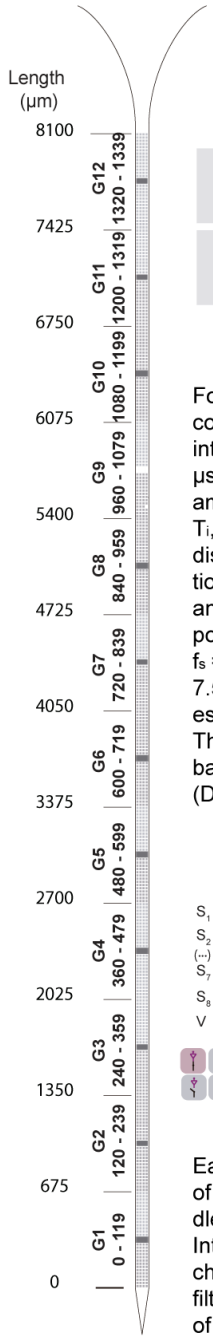

Basic principle of time division multiplexing

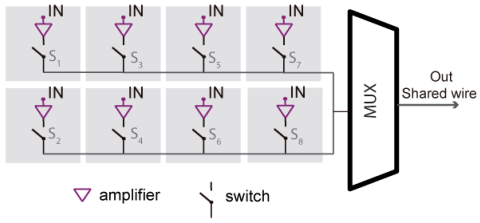

For each electrode the input voltage (IN) is converted to an output current which is integrated for a fixed period of time (T_i = 2.5 µs) over a capacitor (C_i = 15 pF) shared among 8 electrodes in the probe base. After T_i, the voltage on C_i is sampled and then it is discharged for the next cycle. The integration reduces out-of-band noise acting as anti-aliasing filter. Further noise reduction is possible by oversampling each electrode at f_s = 40 kHz (neural signal band is limited to ~ 7.5 kHz, therefore f_s > 15 kHz), wich produces a total multiplexing frequency of 320 kHz. The signal is fed to an integrator, in the base, whose output is demultiplexed (DMUX block).

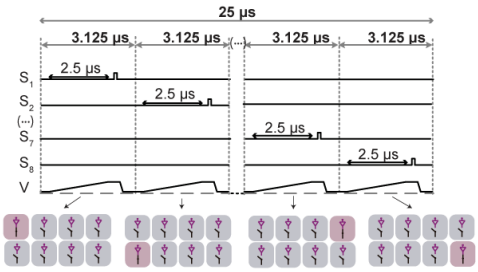

Each reference electrode is made from a bin of 8 electrodes, therefore the circuit handles, in total, 1440 channels. A total of 180 Integrator-DMUX blocks drive the 1440 channels, which are further amplified and filtered on the base, keeping only the band of interest. These signals are then multiplexed and digitized in groups of 20 channels (10-bit successive approximation analog-to-digital converter) by 72 ADCs. Finally, a digital control block is responsible for generating the clocks for the ADCs and the MUX/DMUX blocks. It also serializes the parallel data from all the ADCs to only 6 data lines (Raducanu et al., 2017).

Results

Several recordings were performed with the NeuroSeeker CMOS-based scanning probes *in vivo* to evaluate the viability of these devices. There are 12 groups of electrodes on the probe, which can be individually powered, labelled from G1 to G12, in Box 1 and Figure 1. Each group contains 120 channels: 112 electrodes and 1 local reference in the middle made from a group of 8 electrodes binned together. For each electrode, the user can select the reference type (external or internal), gain, and frequency bandwidth (high-pass cut-off frequency in AP mode or low-pass cut-off frequency in LFP mode). For all recordings, 1277 electrodes were set in the AP band (0.5–7.5 kHz), while 67 were set in the LFP band (1-500 Hz). The LFP electrodes were spaced 20 electrodes apart from one another, which translates to 5 rows, or, given the 22.5 µm pitch of each electrode, 112.5 µm.

Neural recordings

Acute recordings

Figure 1A shows a representative epoch of a recording performed simultaneously within cortex, hippocampus, and thalamus from an anesthetized rat. In this recording, 10 of the 12 groups are in the brain and thus enabled (powered on): 1060 AP mode and 60 LFP mode ones. A subset of traces from electrodes set in AP and LFP mode are shown in Figure 1A (a recording segment of all traces is shown in Supplementary Figure 1). The traces in AP mode are displayed in groups (c1, c2, c3, cg, h1, h2, h3, h4, t1, t2, t3 and t4) that correspond to the location on the probe shaft indicated by the black region in the probe schematic. Moreover, traces of 11 out of 60 LFP mode electrodes are plotted between the group traces. The presence of fast voltage deflections in several traces reveals that the spiking activity of multiple neurons has been detected. Furthermore, the NeuroSeeker probe densely samples the local electric field, providing a detailed description of the spatiotemporal profile of a neuron's extracellular action potential, as shown in Figure 1C.

To evaluate if the data quality deteriorates with increasing number of groups powered, we computed the noise of 212 electrodes (from groups G1 and G2) set in AP mode while enabling more groups along the shank. The noise level for the 212 electrodes using the external reference, with 2 groups and 12 groups powered, is 10.2 ± 0.1 µV and 12.0 ± 0.1 µV, respectively. Additionally, the noise magnitude was computed for the 1012 channels in the brain (half of group 10's electrodes are outside of the brain) using either the external or the internal reference configuration while recording. The measured noise using the external and internal reference is 11.7 ± 0.1 µV and 12.5 ± 0.1 µV, respectively. The noise magnitude computed across these datasets revealed no significant variability. We also measured the noise in saline for the NeuroSeeker probe. The measured noise in saline while powering the same 1012 channels was 9.4 ± 0.1 µV. We compared the noise measured in saline and during acute recordings with a 128-channel probe previously described (Neto et al., 2016). This passive electrode probe has the same configuration, electrode size, and electrode material (titanium nitride) as the CMOS-based probe (impedance magnitude at 1 kHz is around 50 kΩ). The noise value calculated with the 128-channel probe in saline was 2.69 ± 0.02 µV and *in vivo* (*amplifier2015-08-28T20_15_45* in http://www.kampff-lab.org/validating-electrodes/) was 10.40 ± 0.04 µV. Despite the difference in saline (9.4 vs 2.7 µV) the noise difference *in vivo* was small (11.7 vs 10.4 µV) between the CMOS-based probe and the passive 128-channel probe, highlighting the dominance of "biological" noise for *in vivo* extracellular recordings.

Several recordings were performed with different reference configurations and number of active groups. These datasets are available online (http://www.kampff-lab.org/cmos-scanning/) and

summarized in Supplementary Table 1. Figure 1 is derived from one of these recordings, *18_26_30.bin*.

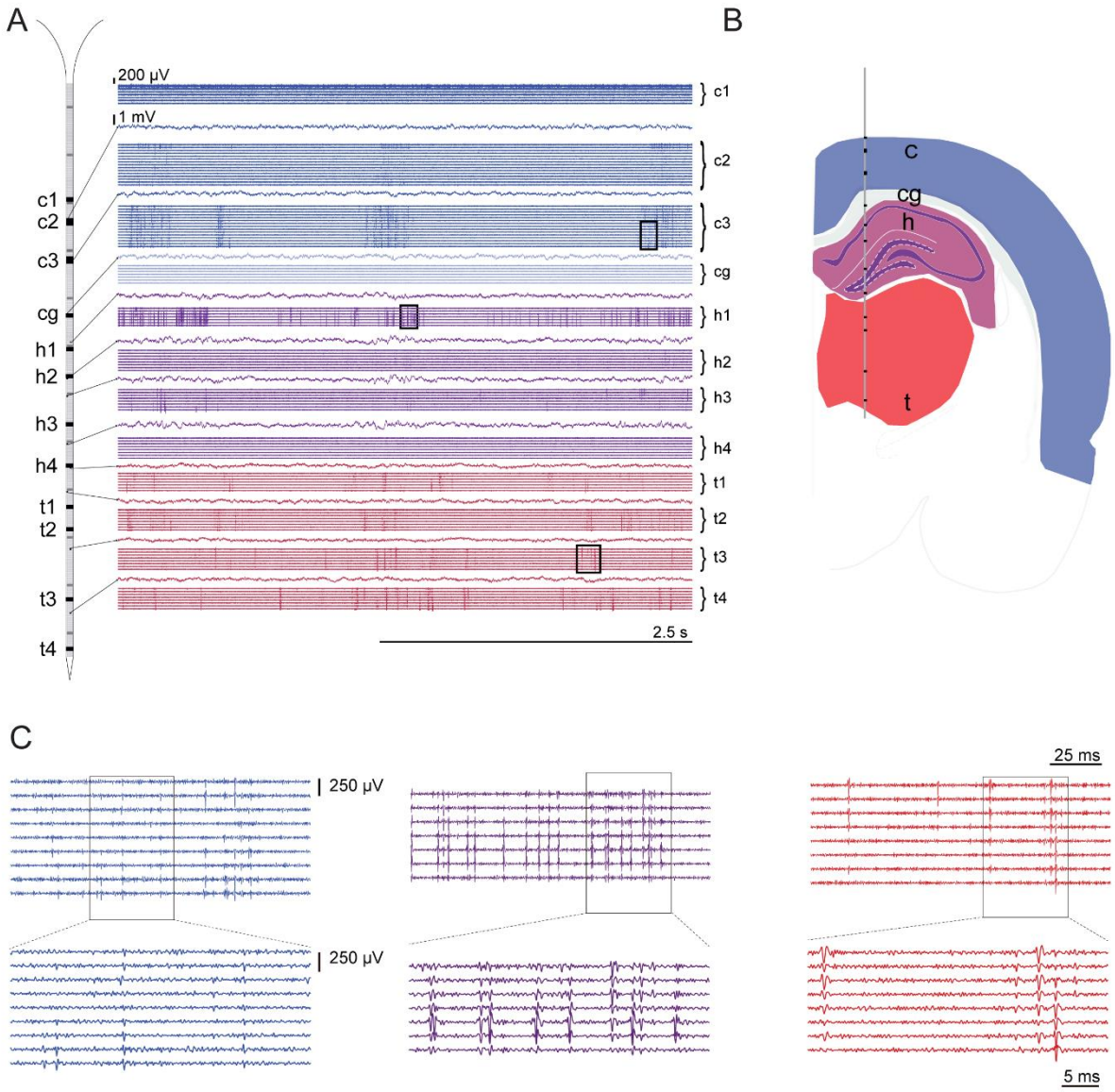

Figure 1. Example of a recording performed with 1120 electrodes simultaneously within cortex, hippocampus, and thalamus from an anesthetized rat. A) 5-s-long LFP and AP traces of a probe spanning multiple brain regions; B) Schematic of coronal slice signalling the group's position shown in A as black blocks. 'c, 'cg', 'h' and 't' denote the anatomic locations of cortex, cingulum, hippocampus, and thalamus, respectively. The estimated probe position was based on the insertion coordinates and physiological signatures. From the point of insertion to the tip, the recording depth was 6.7 mm; C) Short epochs of AP band traces from groups c3, h1, and t3 (color-coded), illustrating the presence of diverse spike waveforms on several electrodes. These sections are highlighted in A by boxed areas on top of traces.

Chronic recordings

We also conducted a set of recordings from chronically implanted animals. Given the high cost and low availability of high density probes, we designed a method that allowed us to extract the CMOS probe from the brain of a chronically implanted animal at the end of the experimental period so that it can be reused for multiple experiments. This required a specially designed probe holder and a series of steps after animal euthanasia to ensure the probe is removed without breaking the fragile shaft. The holder is a two-part design and is shown in Figure 2A, while in Methods we describe a detailed probe recovery technique. We have managed to successfully remove four out of five chronically implanted probes (two dummy and two fully functional). In the case of the unsuccessful attempt, the probe holder exhibited a small angle deflection off the Dorsal-Ventral / Anterior-Posterior plane, even before the cutting of the resin, indicating that the probe had already moved and thus broken while the animal was alive.

In order to showcase the long term recording capabilities and robustness in removal and re-implantation of the probe, we present here recordings from three animals, all implanted with the same probe. In all cases the probe was fully implanted in the brain targeting the parietal cortex and the subcortical regions beneath (see Figure 2B schematics for a description of the anatomical regions the probe was passing through). For the first two animals this resulted in recordings from 1277 electrodes from the AP band and 67 electrodes from the LFP band. In the third animal we had to switch off the bottom two regions of the probe thus creating recordings from 1064 AP electrodes and 56 LFP ones. In all cases, the probe was left in the animal for 4 weeks. Each animal was recorded daily in a freely moving session which ranged between 40 to 70 minutes. Each session generated between 1.7M and 8M spikes per hour of recording. Spikes were represented on groups of adjacent electrodes that ranged in size between 10 and 50 with most of the spikes showing on at least 40 electrodes. We spike sorted some representative sessions to demonstrate the robustness of the recordings over time and our ability to remove the probe from one animal, implant it in another, and still get recordings of the same quality as a new probe. During the spike sorting pipeline (using kilosort (Pachitariu et al., 2016) and t-SNE (Dimitriadis et al., 2016)) we separated the units into two categories. These were the single units and the multi units i.e. the groups with spikes that originated from more than one neurons. Figure 2B shows the position of these units (color coded according to their assignment) on the probe shaft (see Methods on how these positions are calculated). For the first implanted rat we show three recordings, taken 3, 7 and 10 days after surgery. For the second rat we show the first recording taken 3 days after surgery. For the third rat we show a recording taken 7 days after surgery. Figure 2C shows the number of the different types of units over the different recordings. Table 1 summarizes the number of units and number of spikes recorded in each session. The number of detected templates (most of them single units) ranged between 1389 and 633. In (Dimitriadis et al., 2016) we reported that in an under anesthesia session (with a different NeuroSeeker probe) and with 908 electrodes in the brain we detected 579 units, comparable to the unit count we get in these awake experiments. The data show that the probe proved to be a robust recording device, able to detect over 1000 units simultaneously while not showing a significantly worse deterioration of its capacity compared to any other silicon probe over extended periods of recording.

The data also show that multiple use of the same device is possible and does not impact on the quality of the recordings. We note here that the first and third animal implantations were done in a slow manner (over 1 hour for the whole 8 mm length) while the implantation of the second animal

was done in a fast manner (5 minutes for the whole probe). This might be one reason that the second animal recordings show a reduced number of neurons, especially of the clean single unit type (i.e. the neurons closer to the shaft) and of the number of spikes recorded.

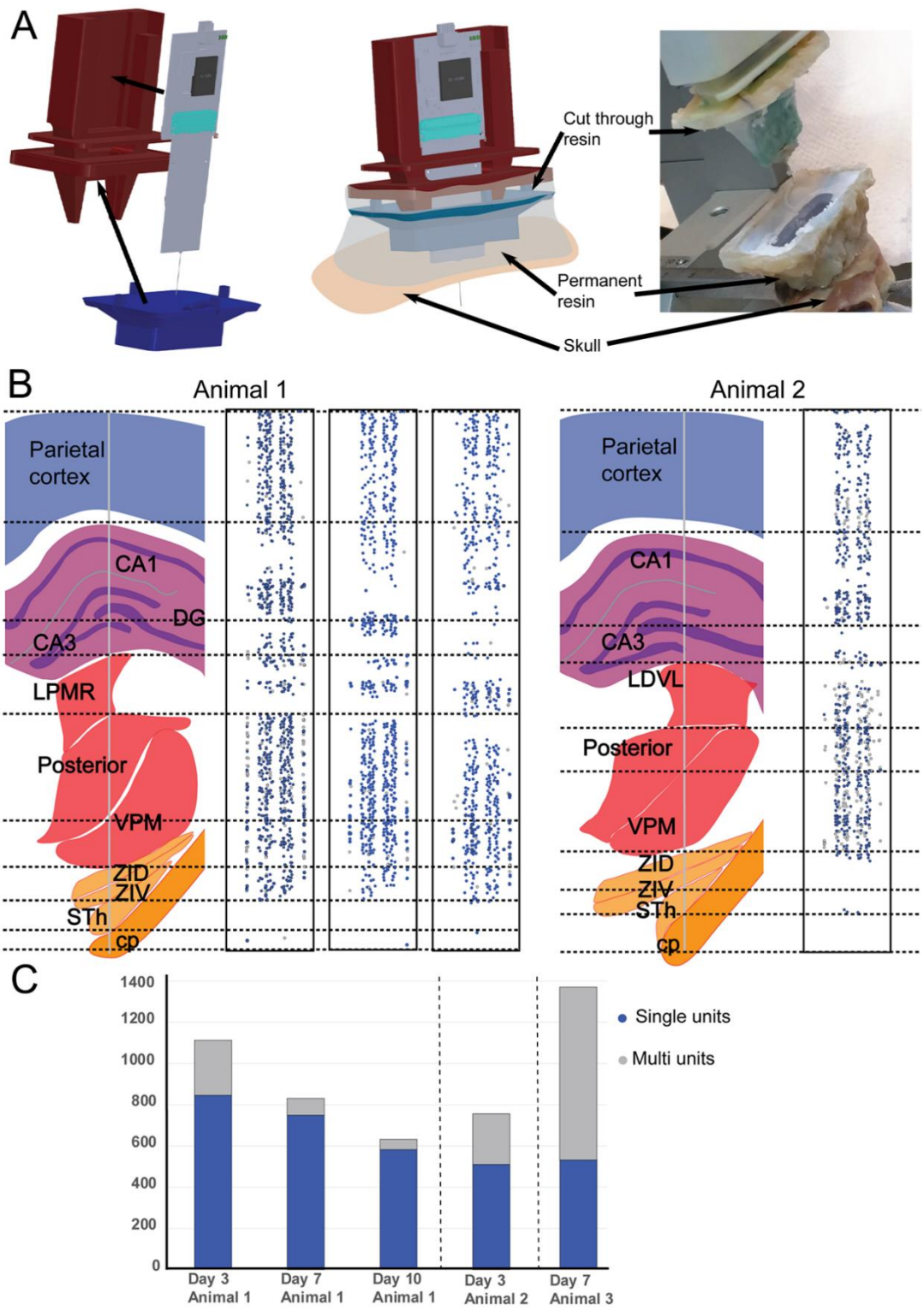

Figure 2. Chronic recordings and probe removal process. A) The processes of inserting the probe before surgery (left), implanting and gluing the probe in place during surgery (middle) and removing the probe by cutting the cut-through resin layer after surgery (right). B) Results from three animals chronically implanted with the same probe (animals 1,2 and 3 implanted in that order). The two anatomy schematics show where the probe was implanted in two of the three animals. The scatter

plots show the position of the recorded units on the probe, each for one recording session. Each dot is a single (blue) or a multi unit (grey) group and the axis are the y and x coordinates of the probe's shaft (not shown to the same scale due to the extremely elongated nature of the shaft). The three position plots of the first animal show recordings done 3, 7 and 10 days after surgery, while the plot for the second animal show the first recording, done on the 3rd day after surgery. C) Cumulative bar chart showing the number of recorded units over days for the three animals (Animals 1 and 2 are the same in B and C). Brain regions: CA1: Cornu Ammonis 1, CA3: Cornu Ammonis 3, DG: Dentate Gyrus, LPMR: Lateral Posterior MedioRostral thalamic nucleus, LDVL: Lateral Dorsal VentroLateral thalamic nucleus: VPM: Ventral Posterior Medial thalamic nucleus, ZID: Zona Incerta Dorsal, ZIV: Zona Incerta Ventral, Sth: Subthalamic nuclei, cp: cerebral penducle

Data visualization

The signal traces presented in Figure 1 are just a small fraction of the total number of electrodes (105 of 1060 electrodes) recorded during an acute experiment (see all voltage traces in Supplementary Figure 1). These ultra-high channel count CMOS scanning probes presented a new challenge for the visualization and analysis of the acquired data. This challenge first appears when the user wants to monitor an ongoing recording, either to assess the signal quality appearing on each electrode or to better position the probe within the desired brain structure(s). Visualizing 1344 time series is difficult, even on an HD monitor with 1080 rows of pixels. Furthermore, rendering voltage vs. time traces, the conventional representation for online physiology signals, is computationally expensive. However, modern graphic processors (GPUs) were specifically designed to parallelize such visualization tasks. We therefore developed a custom visualization pipeline using Bonsai (Lopes et al., 2015) by transferring each buffer of acquired probe data directly to the GPU and then using fragment shaders to render all probe data in real-time. The visualization shown in Figure 3 is a screen capture of one such online visualization in which the voltage signal of each channel is rendered from red to blue (also see Supplementary Movie 1). A neuron's extracellular action potential is detected on many adjacent electrodes, and thus spikes in this visualization appear as a coloured block of red and blue stripes.

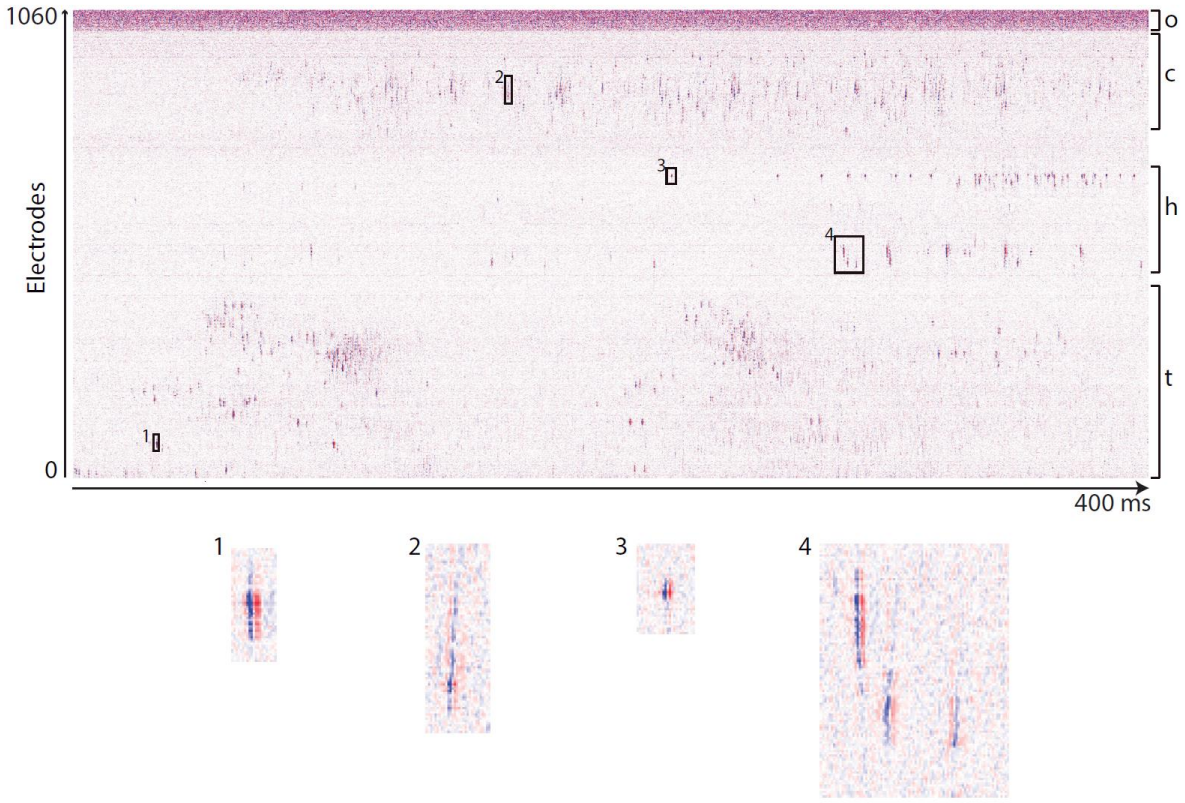

Figure 3. Real time GPU-based visualization of the voltage traces from 1060 electrodes in AP mode during acute recordings under anesthesia. The voltage traces recorded by each electrode (row) are displayed as a color saturation for each 100 microsecond bin (column). Red represents positive voltages (maximum color value represents 150 µV), blue negative voltages (minimum color value represents -150 µV), and white represents voltages near zero. This image shows 400 milliseconds of data recorded simultaneously in cortex, hippocampus and thalamus. 'o': out of the brain, 'c': cortex, 'h': hippocampus and 't': thalamus.

Global vs. local signals

The animals in our chronic recordings were engaged in a foraging task which at the end of each successful trial rewarded them with a chocolate pellet they could access from a nose poke. During their free foraging (in a 1 x 1 m arena) they were recorded by a 120 fps camera. We used this setup to answer whether having access to both a large number of brain regions and to the detailed single neuron spiking information would be advantageous to our understanding of how the brain generated behaviour. We first focused on brain activity around the time of the reward and asked if the multi-regional coverage of the NeuroSeeker probe offered any advantage. The results for animals 2 and 3 can be seen in Figure 4. The figure shows the average firing rates of all neurons (each normalised to itself) over a period of ±8 sec around the reward delivering poke. Compared to the averages around random time points, a regions wide pattern of activity becomes apparent, with different functional areas increasing and/or decreasing their firing rates with an order of succession that seems to hold over animals (given our sample size of two). Taking into account that the different regions targeted by the probe do not have any special anatomical connectivity, the data resulting from our exploratory experimental design allow us to formulate the hypothesis that such patterns of activity might be ubiquitous in the brain with even more regions being part of this

interplay of populational activity modulation. We argue that such global patterns have up to today gone unrecognised due to the limited number of regions standard probes can access. To test the above hypothesis one would need multi shank probes that can access multiple regions of the brain, both superficial and deep. Such probes have started to appear (Chung et al., 2019; Musk and Neuralink, 2019) and one can now use some of these technologies to target multiple regions anywhere in the brain. What these non CMOS probe technologies though compromise on, in order to achieve recording spread, is electrode density.

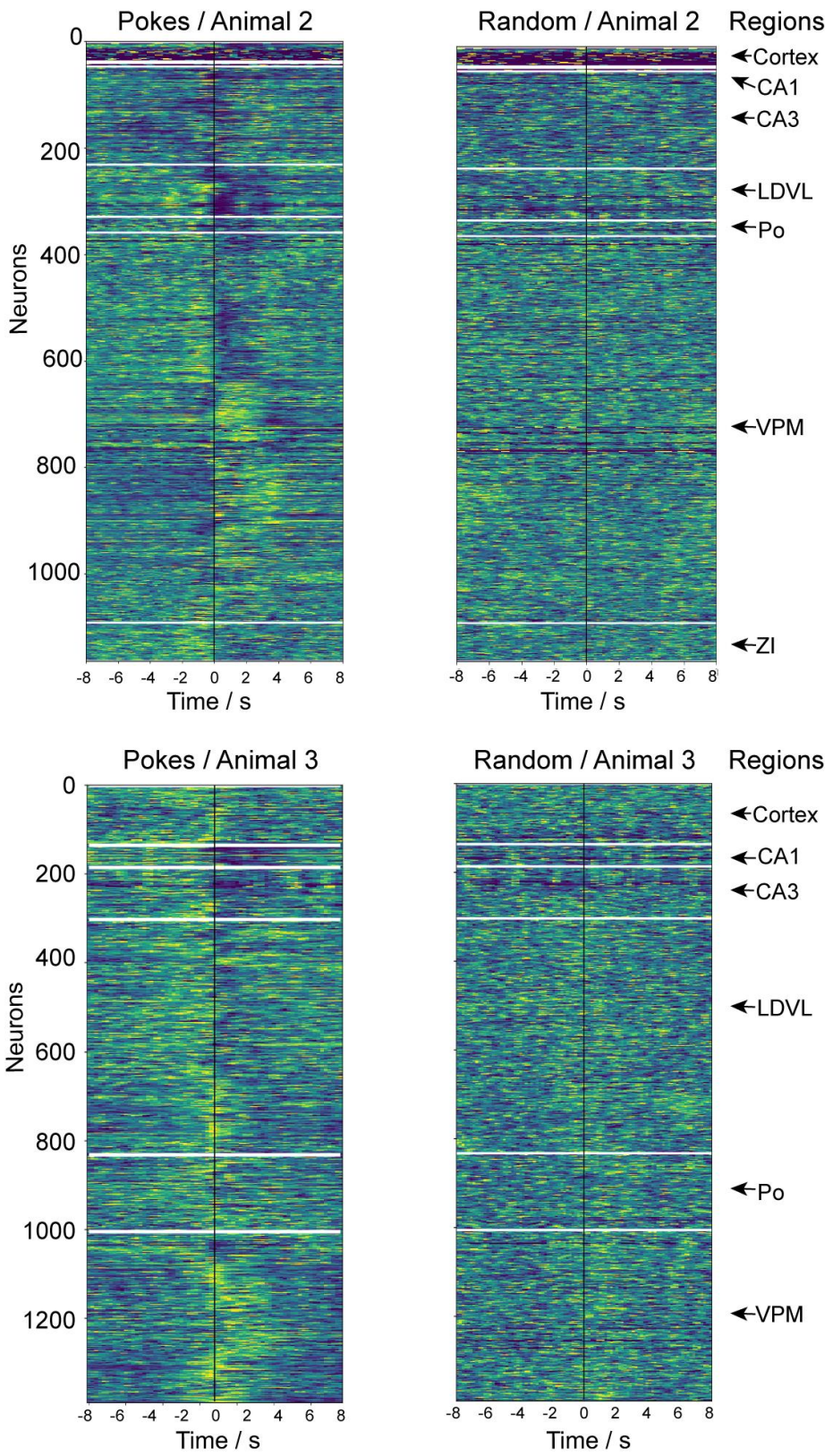

Figure 4. Global patterns of differential firing activity around specific events during a behavior task. Each figure shows the normalised firing rate of each neuron, averaged over trials and sorted in the y axis according to the depth of the neuron in the brain. The rows show the pattern formed in two separate animals (row 1 for animal 2 and row 2 for animal 3, animals are the same as in Figure 2). Column 1 shows the activity around the poking events and column 2 around randomly selected time points over the duration of the recording.

In order to test what a probe with large regional targeting but lower density would record in a comparable data set, we started from our data and decimated the recording electrodes, lowering the electrode density by a factor of 4 and of 16. These densities were chosen so that a 400 electrode probe would be able to target 10 mm with a single shank (factor of 4) and 4 shanks of 10 mm each (factor of 16). We then rerun the spike sorting analysis. A summary of how many neurons each electrode density design managed to detect can be seen in Figure 5 (with more details shown in Table 2). The reduced electrode density significantly diminished the quality of the local information gained. Figure 5 shows that a reduction of density by a factor of 16 resulted in the reduction of all units detected by a factor of more than 6 and of the single units by a factor of more than 10.

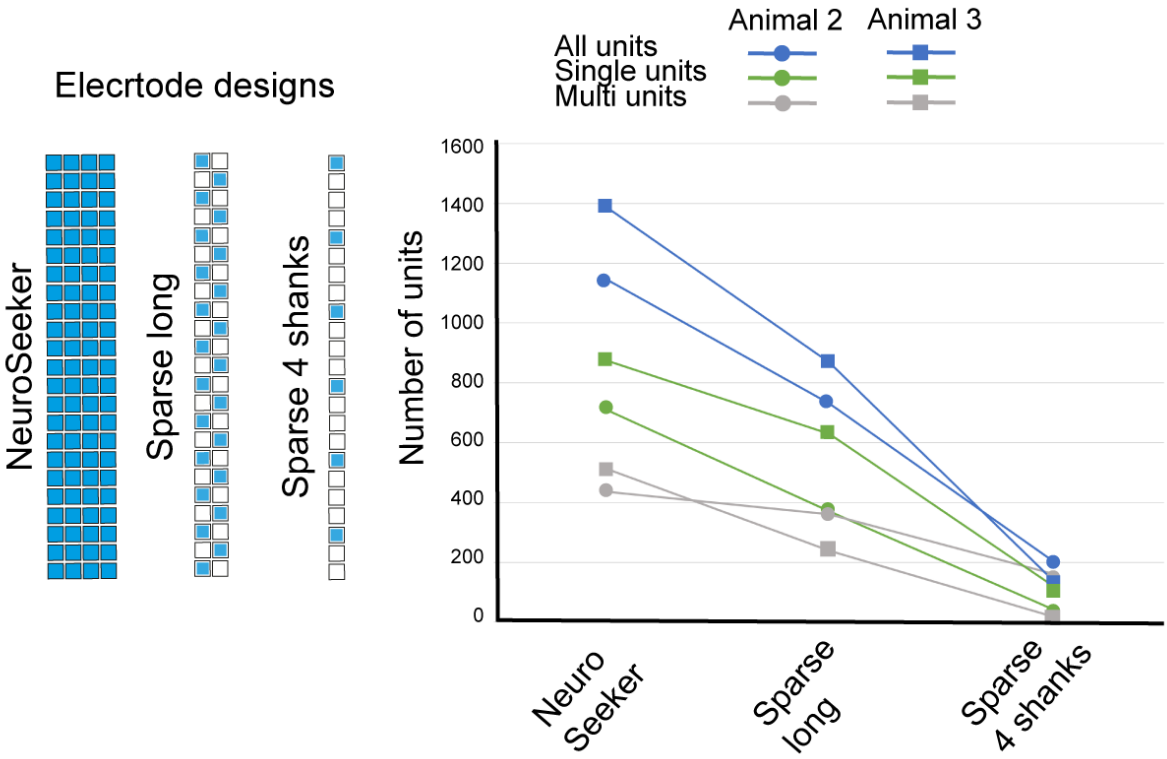

Figure 5. Different electrode densities and the drop in the number of single (green) and multi (grey) units (blue is the total units) in animals 2 and 3. The Sparse long configuration is a reduction of electrode density by 8 and the Sparse 4 shanks one by 16 compared to the original NeuroSeeker electrode design.

We then asked if the extra information arising from the detailed knowledge of single neuron activity would be beneficial in defining brain states that corresponded more accurately with behaviour outcomes. In order to create a preliminary test for this we first defined behavioural states as follows.

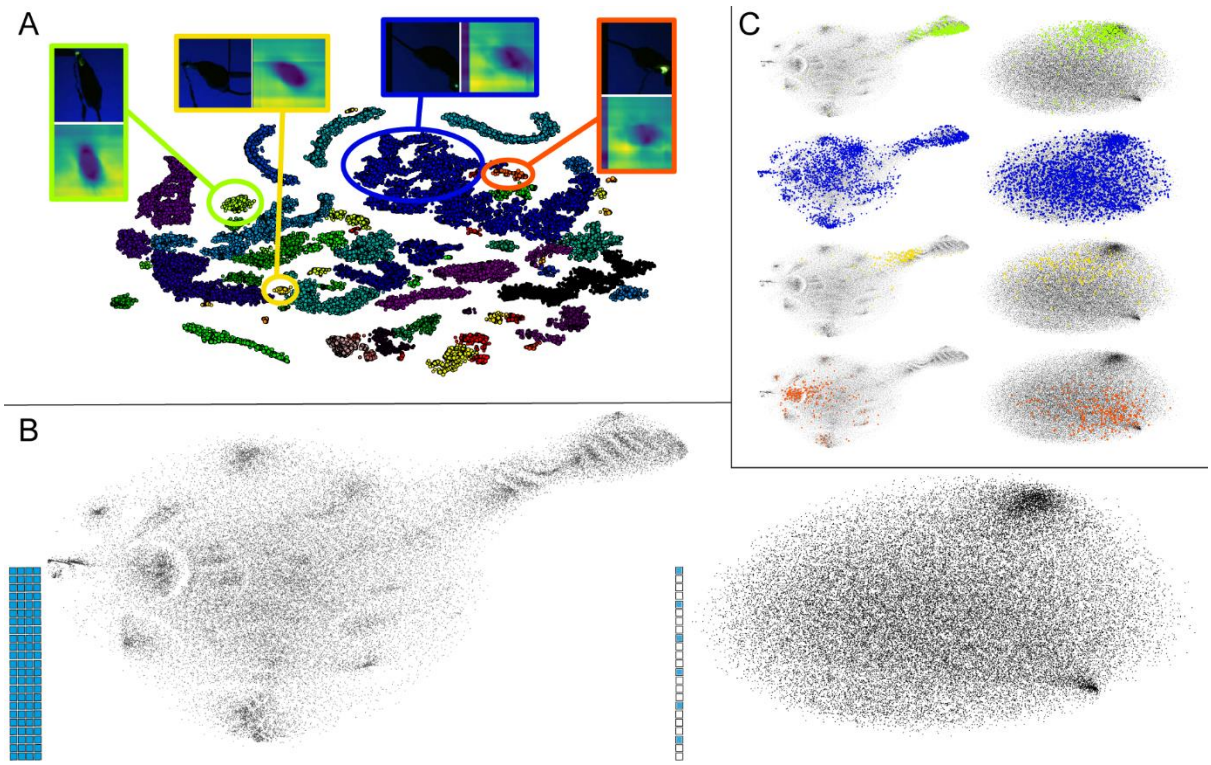

Figure 6. The reduction in the density of the recording electrodes is followed by reduction in the detection of self-similar brain activity patterns. A) The t-SNE dimensionality reduction and DBSCAN clustering results of the cropped and averaged behavioural video. The 4 inserts show a characteristic example of the frames in the 4 marked clusters. The top/left of the insert is the actual frame and the bottom/right the reconstruction of the top 100 PCs (which is what was fed into the t-SNE algorithm). B) The t-SNE embedding of the NeuroSeeker (left) and the Sparse 4 shanks (right) recording (firing rates of all neurons) of that session. C) The same t-SNEs as in B but with the points that cluster in the four clusters in A superimposed.

We cropped the behavioural video around the animal and then subsampled it by averaging every 12 frames (creating a new video of 10 fps). We then run the cropped and subsampled video through a principal component analysis (PCA) algorithm and kept the top 100 components (Figure 6A shows in the 4 inserts 4 average frames and their equivalent reconstructions from the 100 top PCs). We then passed these 100 PCs of all frames to the t-SNE algorithm (Dimitriadis et al., 2018) and finally used DBSCAN to cluster the resulting 2D embedding. Figure 6A shows the results of this process. Each cluster corresponds to a specific combination of the animal's place in the arena and its body posture. The arena had enough unique landmarks that one can easily identify the animal's position in it even in the cropped video. For example, clusters blue and red in Figure 6 are both defined by the times that the animal is at the poke with its body angled at about 120 degrees off the horizontal, but differ by the fact that in the red cluster the animal is rearing so its body shape is more spherical.

Having defined a set of low level behavioural states (described by position and posture) we then followed the same process (PCA and t-SNE) to 2D embed the average firing rates per 100 ms for all neurons. We did this for both the NeuroSeeker density and for the Sparse 4 shanks one (16 times sparser). The results of the embeddings can be seen in Figure 6B. In the case of the NeuroSeeker probe a large percentage of the 100 ms, all neuron firing rates vectors aggregates in self similar regions. In contrast the Sparse 4 shanks embedding shows that a drop in single neuron spiking information makes it impossible to differentiate between unique brain states in an unsupervised learning fashion.

Each point in the embedding of the behaviour video has a corresponding point in the embeddings of the two firing rate embeddings (corresponding to the same 100 ms). The question we wanted to answer was whether the points that cluster together in the behavioural video would have correspondence to local regions in the brain activity embeddings.

Out of the 72 behavioural clusters defined, 66 had no obvious correspondence to sub regions in the brain activity embedding (example of that is the blue cluster in Figure 6C). On the other hand, six of them showed a very localised pattern on the NeuroSeeker brain activity embedding, where similar behaviour corresponded to highly self-similar neural patterns (see Figure 5C showing 3 of these 6 clusters (yellow, red and green)). The second column of Figure 5C shows that this was not the case for the Sparse 4 shanks embedding where these 6 behavioural clusters (3 shown but the other 3 behaved similarly) showed a disperse pattern on the t-SNE embedding. So a drop in density, resulting in a drop in single neuron spiking information also resulted in the loss of the few brain activity regions whose self-similarity corresponded to self-similar behaviour.

Do we need all these electrodes?

Integrating CMOS-based scanning technology into the shaft of an *in* vivo neural probe has now made it possible to drastically increase electrode density. However, given the challenges associated with the volume of data generated by such probes, neuroscientists must decide whether further increases in recording density are actually useful. Current approaches to spike sorting would appear to benefit from higher density probes (Dimitriadis et al., 2018; Moore-Kochlacs, 2016; Rossant et al., 2015). Furthermore, initial results (Jun et al., 2017a) show that increased electrode densities could help compensate for drift in chronic recordings and allow following individual neurons over the course of days and weeks. Finally, CMOS technology enables the fabrication of electrodes much smaller than a neuron's soma and dense enough to capture fine details of a single neuron's extracellular field throughout its dendritic tree (Delgado Ruz and Schultz, 2014; Jia et al., 2018).

Whether useful information is present at these scales, and whether it can contribute to the further understanding of brain function, is an open question. Thus, in order to address whether ultra-high density in neural recordings will be useful, we collected a series of datasets with an ultra-dense probe during anesthesia from many different brain regions (Figure 7A). These data sets are available online (http://www.kampff-lab.org/ultra-dense-survey/) and a summary of them can be seen in Supplementary Table 2.

The ultra-dense probe contains 255 electrodes (and one large reference) with an area of 5 x 5 µm and separated by 1 µm, and was fabricated by IMEC as part of the NeuroSeeker project (see Supplementary Table 3 for a review of the CMOS and ultra-dense passive probes). As shown in Supplementary Figure 2, the probe electrodes have a low impedance value at 1 kHz of 790 ± 100 kΩ. Note that 16 of the 255 electrodes are non-functional because their impedance value at 1kHz is higher than 2 MΩ. The noise magnitude computed in saline for the functional electrodes is 5.09 ± 0.03 µV.

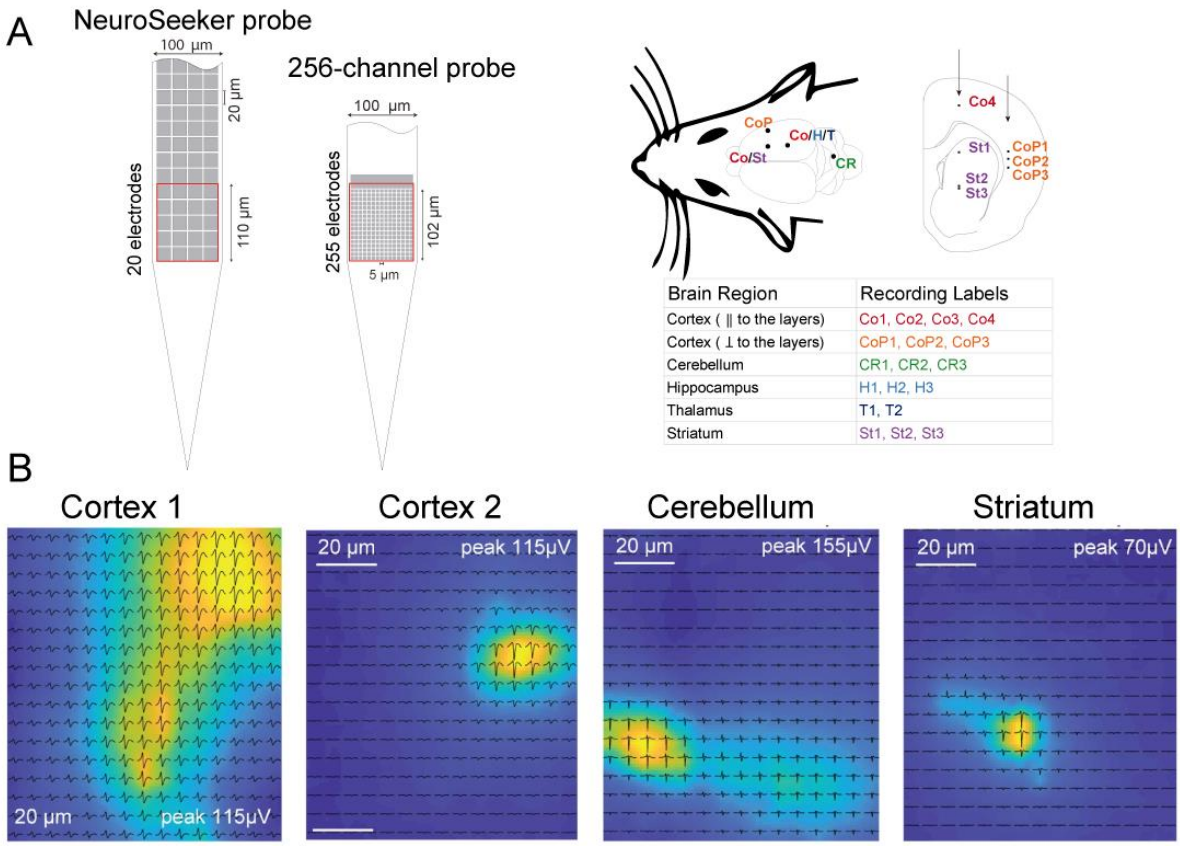

Figure 7. The 256-channel ultra-dense probe packs 255 electrodes in the same area (100 x 102 µm) as 20 electrodes from the NeuroSeeker CMOS scanning probe, a 13x increase in density of electrodes. We conducted four separate penetrations covering five anatomically distinct brain regions and two different orientations (i.e., parallel and perpendicular) with respect to the laminar architecture of cortex, leading to 18 separate recordings.

The data shown in Figure 7B illustrate the ability of this ultra-high-density array of electrodes to detect the activity from the same neuron on several adjacent electrodes thus generating a sort of electrical image of the neuron. This preliminary analysis shows the potential of such densities for the further study of the correlations of this electrical profile with a neuron's position in the brain, its shape or its electrochemical properties. More importantly one can now envision the case of a future CMOS probe with the same resolution as the 255 channels one but with a recording area equal to the NeuroSeeker probe (which would roughly result in a 30,000 channel probe). The operational implications of such technology are admittedly intimidating (30K channels means 4TB of data per hour). Yet maybe connecting single cell morphology and detailed, sub-cellularly resolved, electrical behaviour with network activity from many regions of the brain is a capability the field should serious consider (since the technology is finally here).

Discussion

The NeuroSeeker project is the culmination of a number of efforts to translate major advances in microfabrication into new tools for electrophysiology (Neves et al., 2008; Torfs et al., 2011; Lopez et al., 2013; Jun et al., 2017b; Raducanu et al., 2017; Herbawi et al., 2018; Dorigo et al., 2018). The project has produced a device with multiplexing electrode scanning circuitry within the thin shaft of an implantable neural probe, which provides the highest number of simultaneous outputs for a single shaft *in vivo* extracellular recording device ever achieved.

Here we report that the integrated circuitry of the NeuroSeeker probe does not have an adverse effect on its ability to record neural activity during both acute and chronic recordings. We show that when compared to a passive probe with the same electrode configuration, the NeuroSeeker probe offers simultaneous recordings from >1000 electrodes with similar signal-to-noise ratio. We also show that the probe can be used in long term chronic experiments with a signal deterioration over time comparable to other silicon based probes. Finally, we demonstrate that the probe is both mechanically and electrically robust enough to be removed at the end of a chronic experiment and be reused without any loss of signal quality. Given all this, we propose that integrating on-shank scanning circuitry is not only a promising technology for creating ultra-high density *in vivo* probes, but will, at the very least, allow the simultaneous recording from the entire probe with a density sufficient for accurate spike sorting.

Of course, the promise of such high-density, large electrode count probe designs, with their capability to scale to even larger numbers and densities, offers more than simply increasing spike sorting accuracy; they make it possible to simultaneously extract information from the brain on three different scales. At the single neuron level, high densities provide valuable information about cell type and signal propagation throughout the dendritic tree, which can help address the underlying single cell computation. At the level of the local circuit, recording hundreds of neurons simultaneously from a given functional region (here we record from more than 200 per region) is required to test many major hypotheses in systems neuroscience, e.g. the canonical circuit, the engram, or hebbian learning. At the level of the global network, recording from a number of regions throughout the brain allows studies of how the brain as a large network of functionally and anatomically diverse regions generates complex behavior. A combination of these two capabilities, we argue, is also indispensable for executing exploratory experiments, designed not to answer a specific hypothesis but to rather generate a range of new ones (maybe previously not thought of), something the field of neuroscience might find more rewarding than currently believed. The results we present here demonstrate a new technology that can scale to higher electrode counts with the same, or higher, density of electrodes. Future devices, which distribute dense electrode groups throughout the brain are possible, and clearly worth exploring, also being one of the major aims of large neuroscience projects like the NIH Brain Initiative (Koroshetz et al., 2018).

The number of simultaneously recorded electrodes of the NeuroSeeker probe created new challenges for previously simple aspects of an experiment, e.g. online data monitoring. We also present here a GPU-based method for generating a real-time visualization of the very large data sets generated by these probes. This greatly facilitates the control of an ongoing experiment and provides an intuitive overview of large scale structures present in the spiking activity recorded by the probe, which often spans multiple distinct anatomical and functional brain regions.

Finally, the high costs associated with CMOS development necessitate a large initial investment to produce just a small number of prototype devices. However, the promise of modern CMOS production scaling is that, after an expensive development phase, a large number of equivalent devices can be produced at a tiny fraction of the initial costs. The recent CMOS-based neural probe prototyping efforts, such as NeuroSeeker, have resulted in truly revolutionary devices for neurophysiology. However, a true revolution in neuroscience will only come when these devices are available in large numbers, to the entire community, for the price of a spool of tungsten wires.

Methods

Animal surgeries

All experiments were conducted with Lister Hooded rats ranging between 400 g to 700 g of both sexes. For both acute and chronic surgeries, the animals were anesthetized, placed in a stereotaxic frame and undergone a surgical procedure to remove the skin and expose the skull above the targeted brain region. For the acute surgeries we used urethane (1.6 g/kg, IP) anesthesia, while for the chronic ones we used isoflurane gas anesthesia (2% v/v). At the initial stage of each surgery the animal was also injected with atropine (0.05 mg/kg), temgesic (20 µg/kg, SC) and rimadyl (5 mg/kg, SC). Small craniotomies (about 1 mm in diameter) were performed above the target area. During the surgeries equipment for monitoring the animals' body temperature and a video system for guiding probe insertion (Neto et al., 2016) was used. The targeted insertion coordinates were scaled according to the size of each animal's skull. We measured the distance between bregma (B) and interaural line (IA) for all animals to find the ratio between the animal skull and the reference skull (B – IA = 9 mm) generated as part of the 3D atlas described in (Dimitriadis et al., 2014). Finally, we adapted the insertion coordinates for targeting specific brain regions with the use of the 3D atlas. Animal experiments were approved by the local ethical review committee and conducted in accordance with Home Office personal and project (I19EFD9C9; 70/8116) licenses under the UK Animals (Scientific Procedures) 1986 Act.

Recordings

The CMOS-based probes are assembled on a PCB where the reference (REF) and ground (GND) wires are connected. The recording system consists of a headstage, which configures and calibrates the probe and serializes probe data, a microcoax cable and the base station board with a deserializer chip which connects to a commercial FPGA development board (Xilinx KC705). The computer used for controlling the NeuroSeeker system is connected to the FPGA board via a 1000 kBps-T Ethernet card. This recording system together with the FPGA code and low level C drivers for FPGA - computer communication were developed by IMEC. The FPGA code and the C drivers remain closed source. The protocol for the communication with the low level C drivers for the acquisition and saving of the data and subsequent visualization was implemented in Bonsai. Both Bonsai and the specific NeuroSeeker communication protocol are open source (Bonsai, 2017; Lopes et al., 2015). The CMOS extracellular signals were sampled at 20 kHz with a 10-bit resolution.

Due to the small diameter of the microcoax cable and the size of the behaviour arena there was no requirement for the use of a commutator during the freely moving animal recordings. No cable tension or significant torsion ever developed during the 1-1.5 hour long experimental sessions. The behaviour arena is a 1 x 1 m box with a back projection glass surface as floor onto which a computer projects imagery at a frame rate of 120 Hz. A grasshopper 3 (FLIR) camera is recording the movements of the rat in the arena, also at 120 Hz, while the controlling computer system is live tracking the animal generating x, y positions for each frame.

For the 256-channel probe recordings we used the Open Ephys (http://www.open-ephys.org/) acquisition board along with two RHD2000 128-channel amplifier boards that amplify and digitally multiplex the extracellular electrodes (Intan Technologies). Extracellular signals in a frequency band of 0.1–7,500 Hz were sampled at 20 kHz with 16-bit resolution and were saved in a raw binary format for subsequent offline analysis using Bonsai.

Impedance measurements

For the 256-channel probe, impedance tests (at 1 kHz) were performed using a protocol implemented by the RHD2000 series chip (Intan Technologies) with the electrodes placed in a dish with sterile PBS, 1 mM, pH 7.4 and a reference electrode, Ag-AgCl wire (Science Products GmbH, E-255).

Probe removal

The probe removal from a chronic implantation starts by aligning the rat's head (after euthanasia) with the stereotactic coordinates system. This was done by making sure the probe holder's top surface is parallel to the Anterior-Posterior (AP) / Medial-Lateral (ML) plane of the stereotaxic frame. To achieve this, we make sure this plane is perpendicular to gravity using a spirit level. We then make sure the same thing is true for the rat's head in the stereotaxic frame, i.e. the top surface of the probe's holder is also perpendicular to gravity (using again a spirit level). This step follows from the fact that during probe implantation the probe was held by the stereotaxic frame (while glued on the rat's skull) in such a way that it's top surface was parallel to the frame's AP/ML plane, so by realigning those two planes we bring the probe back to the original position it was implanted in respect to the Dorsal-Ventral (DV) movement of the stereotaxic frame's arm. After alignment, we connect the probe holder to the frame's arm, and then cut through the thin layer of resin (that is kept away from the probe by the tapered skirt), thus separating the part that stays attached onto the head and the part that holds the probe. Then we slowly remove the detached probe by withdrawing the stereotaxic frame's arm. The alignment of the head and the connection of the arm to the still attached probe holder is of importance since any tension between the head and the frame's arm due to misalignment will be released after the cutting of the resin in the form of a movement of the head in respect to the arm resulting in the breaking of the probe shaft. After removal a series of trypsin and ddH_2O cleaning cycles were undertaken until, under a microscope, no organic or salt residues could be seen on the probe's shaft.

Analysis

For the analysis, the CMOS-based probe recordings were filtered with a band-pass of 500-3,500 Hz and saved in binary format using a Bonsai interface. When the external reference was selected, to diminish the effect of artefacts shared across all channels, we subtracted the median signal within each group across the recording electrodes from the respective group.

For the reconstruction of a unit's position on the probe (for the results shown in Figure 3) we used a weighted (according to peak to peak amplitude (PPA)) average of the positions of the electrodes that showed a significant deviation from baseline on the average spike waveform. That is, we selected the electrode with the highest PPA at the time around 0 of a unit's spike template, found all other electrodes whose PPA was over a threshold and then moved the position of the unit from the highest electrode's position towards the other relevant electrodes in a linearly weighted manner according to their PPAs.

For the firing rate activity time locked to an event (trial pokes or randomly selected time points) we first calculated the firing rates of all neurons by summing all of the spikes of each neuron found in a bin of 8.3 ms (equal to one frame of the 120 fps camera we have been using to record the animals' behavior). We then further averaged these firing rates with a moving window of 30 (giving firing rates of 250 ms resolution). We then took 32 bins before and 32 bins after each event (±8 sec) and averaged those firing rate time series together. For animal 2 there were 42 poke events and for

animal 3 49. We used the same number of events to create the average around random time points. The resulting event time locked firing rates were then normalised individually to range between 0 and 1.

For the t-SNE embeddings of the firing rates, we first created average firing rates as above but with a 100 ms window (averaging 12 frames). We then run PCA on the number-of-electrodes X number-of-windows matrix and kept the top 40 principal components (describing 13% of the NeuroSeeker's data variance and 33% of the Sparse 4 shank's one). We finally used t-SNE to embed them in a 2D space. This was run with a perplexity of 100, a theta of 0.3, an eta of 200, exaggeration of 12 and 4000 iterations.

For the video embedding and clustering we first cropped the video around the rat (cropped frame size = 250 x 250 pixels), then averaged every 12 frames (creating the same 100 ms window per data point as above), rescaled to 80 X 80 pixels, greyscaled and flattened. The resulting 6400 X number-of-windows matrix of frames was then run through PCA. We kept the top 100 PCs (95% explained variance) and put those through a t-SNE algorithm with the same settings as above. The DBSCAN algorithm that was run on the resulting embedding had an epsilon of 0.025 and a minimum samples of 40.

For the 256-channel probes, a third order Butterworth filter with a band-pass of 250-9,500 Hz (95% of the Nyquist frequency) was used in the forward-backward mode. The noise magnitude was computed as an estimate of the background noise, σ_{Median} = median(|signal(t)|/0.6745), of each filtered voltage-time trace during 5 seconds. Some results were represented as mean ± standard deviation.

Acknowledgments

Joana Neto was supported by the fellowship SFRH/BD/76004/2011 from Fundação para a Ciência e Tecnologia, Portugal.

Susu Chen was funded by the Wellcome Trust as a Sir Henry Wellcome postdoctoral fellow.

This work was supported by funding from the European Union's Seventh Framework Programme (FP7/2007-2013) under grant agreement nr. 600925 (NeuroSeeker), by the Bial Foundation (Grant 190/12) and by the Hungarian National Brain Research Program 2017_1.2.1-NKP-2017-00002.

References

Berenyi, A., Somogyvari, Z., Nagy, A.J., Roux, L., Long, J.D., Fujisawa, S., Stark, E., Leonardo, A., Harris, T.D., and Buzsaki, G. (2014). Large-scale, high-density (up to 512 channels) recording of local circuits in behaving animals. J. Neurophysiol. *111*, 1132–1149.

Blanche, T.J., Spacek, M.A., Hetke, J.F., and Swindale, N.V. (2005). Polytrodes: high-density silicon electrode arrays for large-scale multiunit recording. J. Neurophysiol. *93*, 2987–3000.

Buzsáki, G., Stark, E., Berényi, A., Khodagholy, D., Kipke, D.R., Yoon, E., and Wise, K.D. (2015). Tools for Probing Local Circuits: High-Density Silicon Probes Combined with Optogenetics. Neuron *86*, 92–105.

Chung, J.E., Joo, H.R., Fan, J.L., Liu, D.F., Barnett, A.H., Chen, S., Geaghan-Breiner, C., Karlsson, M.P., Karlsson, M., Lee, K.Y., et al. (2019). High-Density, Long-Lasting, and Multi-region Electrophysiological Recordings Using Polymer Electrode Arrays. Neuron *101*, 21-31.e5.

Delgado Ruz, I., and Schultz, S.R. (2014). Localising and classifying neurons from high density MEA recordings. J. Neurosci. Methods *233*, 115–128.

Dimitriadis, G., Fransen, A.M.M., and Maris, E. (2014). Sensory and cognitive neurophysiology in rats, Part 1: Controlled tactile stimulation and micro-ECoG recordings in freely moving animals. J. Neurosci. Methods *232*, 63–73.

Dimitriadis, G., Neto, J., and Kampff, A. (2016). T-SNE visualization of large-scale neural recordings.

Dimitriadis, G., Neto, J.P., and Kampff, A.R. (2018). t-SNE Visualization of Large-Scale Neural Recordings. Neural Comput. *30*, 1750–1774.

Dorigo, D.D., Moranz, C., Graf, H., Marx, M., Wendler, D., Shui, B., Herbawi, A.S., Kuhl, M., Ruther, P., Paul, O., et al. (2018). Fully Immersible Subcortical Neural Probes With Modular Architecture and a Delta-Sigma ADC Integrated Under Each Electrode for Parallel Readout of 144 Recording Sites. IEEE J. Solid-State Circuits 1–15.

Dugué, L., Marque, P., and VanRullen, R. (2011). The phase of ongoing oscillations mediates the causal relation between brain excitation and visual perception. J. Neurosci. Off. J. Soc. Neurosci. *31*, 11889–93.

Herbawi, A.S., Christ, O., Kiessner, L., Mottaghi, S., Hofmann, U.G., Paul, O., and Ruther, P. (2018). CMOS Neural Probe With 1600 Close-Packed Recording Sites and 32 Analog Output Channels. J. Microelectromechanical Syst. 1–12.

Jia, X., Siegle, J., Bennett, C., Gale, S., Denman, D., Koch, C., and Olsen, S. (2018). High-density extracellular probes reveal dendritic backpropagation and facilitate neuron classification.

Jun, J., Mitelut, C., Lai, C., Gratiy, S.L., Anastassiou, C.A., and Harris, T.D. (2017a). Real-time spike sorting platform for high-density extracellular probes with ground-truth validation and drift correction. BioRxiv 1–29.

Jun, J.J., Steinmetz, N.A., Siegle, J.H., Denman, D.J., Bauza, M., Barbarits, B., Lee, A.K., Anastassiou, C.A., Andrei, A., Aydın, Ç., et al. (2017b). Fully integrated silicon probes for high-density recording of neural activity. Nature *551*, 232–236.

Koroshetz, W., Gordon, J., Adams, A., Beckel-Mitchener, A., Churchill, J., Farber, G., Freund, M., Gnadt, J., Hsu, N.S., Langhals, N., et al. (2018). The State of the NIH BRAIN Initiative. J. Neurosci. *38*, 6427–6438.

Lopes, G., Bonacchi, N., Frazão, J., Neto, J.P., Atallah, B. V, Soares, S., Moreira, L., Matias, S., Itskov, P.M., Correia, P.A., et al. (2015). Bonsai: an event-based framework for processing and controlling data streams. Front. Neuroinformatics *9*, 7.

Lopez, C.M., Andrei, A., Mitra, S., Welkenhuysen, M., Eberle, W., Bartic, C., Puers, R., Yazicioglu, R.F., and Gielen, G. (2013). An implantable 455-active-electrode 52-channel CMOS neural probe. In 2013 IEEE International Solid-State Circuits Conference Digest of Technical Papers, (IEEE), pp. 288–289.

Lopez, C.M., Mitra, S., Putzeys, J., Raducanu, B., Ballini, M., Andrei, A., Severi, S., Welkenhuysen, M., Van Hoof, C., Musa, S., et al. (2016). A 966-electrode neural probe with 384 configurable channels in

0.13µm SOI CMOS. In 2016 IEEE International Solid-State Circuits Conference (ISSCC), (IEEE), pp. 392–393.

Moore-Kochlacs, C.E. (2016). Extracellular electrophysiology with close-packed recording sites: spike sorting and characterization. Boston University.

Musk, E., and Neuralink (2019). An integrated brain-machine interface platform with thousands of channels (Neuroscience).

Najafi, K., and Wise, K.D. (1986). An implantable multielectrode array with on-chip signal processing. IEEE J. Solid-State Circuits *21*, 1035–1044.

Najafi, K., Wise, K.D., and Mochizuki, T. (1985). A high-yield IC-compatible multichannel recording array. IEEE Trans. Electron Devices *32*, 1206–1211.

Neto, J.P., Lopes, G., Frazão, J., Nogueira, J., Lacerda, P., Baião, P., Aarts, A., Andrei, A., Musa, S., Fortunato, E., et al. (2016). Validating silicon polytrodes with paired juxtacellular recordings: method and dataset. J. Neurophysiol. *116*, 892–903.

Neves, H.P., Torfs, T., Yazicioglu, R.F., Aslam, J., Aarts, A.A., Merken, P., Ruther, P., and Van Hoof, C. (2008). The NeuroProbes project: a concept for electronic depth control. Conf. Proc. Annu. Int. Conf. IEEE Eng. Med. Biol. Soc. IEEE Eng. Med. Biol. Soc. Annu. Conf. *2008*, 1857.

Obien, M.E.J., Deligkaris, K., Bullmann, T., Bakkum, D.J., and Frey, U. (2015). Revealing neuronal function through microelectrode array recordings. Front. Neurosci. *8*, 423.

Pachitariu, M., Steinmetz, N., Kadir, S., Carandini, M., and Harris, K.D. (2016). Kilosort: realtime spike-sorting for extracellular electrophysiology with hundreds of channels.

Raducanu, B.C., Yazicioglu, R.F., Lopez, C.M., Ballini, M., Putzeys, J., Wang, S., Andrei, A., Welkenhuysen, M., Van Helleputte, N., Musa, S., et al. (2016). Time multiplexed active neural probe with 678 parallel recording sites. In European Solid-State Device Research Conference, (IEEE), pp. 385–388.

Raducanu, B.C., Yazicioglu, R.F., Lopez, C.M., Ballini, M., Putzeys, J., Wang, S., Andrei, A., Rochus, V., Welkenhuysen, M., Helleputte, N. van, et al. (2017). Time Multiplexed Active Neural Probe with 1356 Parallel Recording Sites. Sensors *17*, 2388.

Rios, G., Lubenov, E. V., Chi, D., Roukes, M.L., and Siapas, A.G. (2016). Nanofabricated Neural Probes for Dense 3-D Recordings of Brain Activity. Nano Lett. *16*, 6857–6862.

Rossant, C., Kadir, S.N., Goodman, D.F.M., Schulman, J., Belluscio, M., Buzsaki, G., and Harris, K.D. (2015). Spike sorting for large, dense electrode arrays (Cold Spring Harbor Labs Journals).

Ruther, P., and Paul, O. (2015). New approaches for CMOS-based devices for large-scale neural recording. Curr. Opin. Neurobiol. *32*, 31–37.

Scholten, K., and Meng, E. (2016). Electron-beam lithography for polymer bioMEMS with submicron features. Microsyst. Nanoeng. *2*, 16053.

Scholvin, J., Kinney, J.P., Bernstein, J.G., Moore-Kochlacs, C., Kopell, N., Fonstad, C.G., and Boyden, E.S. (2016). Close-packed silicon microelectrodes for scalable spatially oversampled neural recording. IEEE Trans. Biomed. Eng. *63*, 120–130.

Seymour, J.P., Wu, F., Wise, K.D., and Yoon, E. (2017). State-of-the-art MEMS and microsystem tools for brain research. Microsyst. Nanoeng. *3*, 16066.

Shobe, J.L., Claar, L.D., Parhami, S., Bakhurin, K.I., and Masmanidis, S.C. (2015). Brain activity mapping at multiple scales with silicon microprobes containing 1,024 electrodes. J. Neurophysiol. *114*, 2043–2052.

Steinmetz, N.A., Koch, C., Harris, K.D., and Carandini, M. (2018). Challenges and opportunities for large-scale electrophysiology with Neuropixels probes. Curr. Opin. Neurobiol. *50*, 92–100.

Stevenson, I. (2017). Tracking Advances in Neural Recording.

Stevenson, I.H., and Kording, K.P. (2011). How advances in neural recording affect data analysis. Nat. Neurosci. *14*, 139–142.

Torfs, T., Aarts, A. a. A., Erismis, M.A., Aslam, J., Yazicioglu, R.F., Seidl, K., Herwik, S., Ulbert, I., Dombovari, B., Fiath, R., et al. (2011). Two-dimensional multi-channel neural probes with electronic depth control. IEEE Trans. Biomed. Circuits Syst. *5*, 403–412.

Wise, D.K., and Ji, J. (1992). An Implantable CMOS Circuit Interface for Multiplexed Microelectrode Recording Arrays. IEEE J. Solid-State Circuits *27*, 433–443.

Wise, K.D., and Najafi, K. (1991). Microfabrication techniques for integrated sensors and microsystems. Science *254*, 1335–1342.

	1st Animal / Day 3	1st Animal / Day 7	1st Animal / Day 10	2nd Animal / Day 3	3rd Animal / Day 7
Single units	846	750	582	512	513
Multi units	267	81	51	246	876
Total units	1113	831	633	756	1389
Spikes	3,586,965	2,610,528	2,536,517	1,449,147	22,155,583
Recording time	40:30	46:58	1:00:05	49:28	2:36:24
Spikes / hour	5,380,447	3,332,588	2,536,517	1,774,465	8,521,378

Table 1. A summary of the number of units and number of spikes recorded during five representative sessions

Animal 2	NeuroSeeker	Sparse Long	Sparse Long percentages	Sparce 4 Shanks	Sparce 4 Shanks percentages
Total units	1147	731	0.64	205	0.18
Multi units	436	361	0.83	162	0.37
Single units	711	370	0.52	43	0.06
% multi units	0.38	0.49		0.79	
% single units	0.62	0.51		0.21	

Animal 3	NeuroSeeker	Sparse Long	Sparse Long percentages	Sparce 4 Shanks	Sparce 4 Shanks percentages
Total units	1389	868	0.62	140	0.10
Multi units	876	629	0.72	121	0.14
Single units	513	239	0.47	19	0.04
% multi units	0.63	0.72		0.86	
% single units	0.37	0.28		0.14	

Table 2. Detailed results on the number of single, multi an total units detected in two animals with the different probe electrode densities.